Journal of proteome research

Article

pubs.acs.org/jpr

Cd^{2+}-Induced Alteration of the Global Proteome of Human Skin Fibroblast Cells

John M. Prins,[†] Lijuan Fu,[‡] Lei Guo,[‡] and Yinsheng Wang*[,†,‡]

[†]Department of Chemistry and [‡]Environmental Toxicology Graduate Program, University of California, Riverside, California 92521-0403, United States

Supporting Information

ABSTRACT: Cadmium (Cd^{2+}) is a toxic heavy metal and a well-known human carcinogen. The toxic effects of Cd^{2+} on biological systems are diverse and thought to be exerted through a complex array of mechanisms. Despite the large number of studies aimed to elucidate the toxic mechanisms of action of Cd^{2+}, few have been targeted toward investigating the ability of Cd^{2+} to disrupt multiple cellular pathways simultaneously and the overall cellular responses toward Cd^{2+} exposure. In this study, we employed a quantitative proteomic method, relying on stable isotope labeling by amino acids in cell culture (SILAC) and LC−MS/MS, to assess the Cd^{2+}-induced simultaneous alterations of multiple cellular pathways in cultured human skin fibroblast cells. By using this approach, we were able to quantify 2931 proteins, and 400 of them displayed significantly changed expression following Cd^{2+} exposure. Our results unveiled that Cd^{2+} treatment led to the marked upregulation of several antioxidant enzymes (e.g., metallothionein-1G, superoxide dismutase, pyridoxal kinase, etc.), enzymes associated with glutathione biosynthesis and homeostasis (e.g., glutathione S-transferases, glutathione synthetase, glutathione peroxidase, etc.), and proteins involved in cellular energy metabolism (e.g., glycolysis, pentose phosphate pathway, and the citric acid cycle). Additionally, we found that Cd^{2+} treatment resulted in the elevated expression of two isoforms of dimethylarginine dimethylaminohydrolase (DDAH I and II), enzymes known to play a key role in regulating nitric oxide biosynthesis. Consistent with these findings, we observed elevated formation of nitric oxide in human skin (GM00637) and lung (IMR-90) fibroblast cells following Cd^{2+} exposure. The upregulation of DDAH I and II suggests a role of nitric oxide synthesis in Cd^{2+}-induced toxicity in human cells.

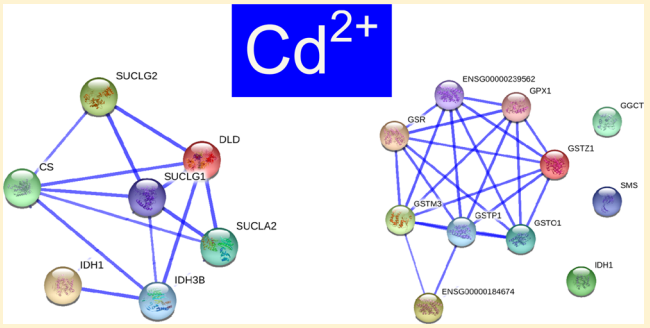

KEYWORDS: *Cd^{2+}, mass spectrometry, protein quantitation, stable isotope labeling by amino acids in cell culture, reactive oxygen species, nitric oxide synthesis*

INTRODUCTION

Owing to its extensive use in industrial processes, cadmium is a toxic heavy metal that is widely distributed throughout the environment.[1,2] Cd^{2+} is one of the leading toxic agents detected in the environment according to the Agency for Toxic Substances and Disease Registry.[3] Being an element, Cd^{2+}, once it becomes deposited into ecosystems, remains there indefinitely because it cannot be broken down further into less toxic substances. Environmental Cd^{2+} can enter biological systems through ingestion, inhalation, and dermal contact.[1,2]

Cd^{2+} is a well-known human carcinogen, and human exposure to Cd^{2+} can lead to the development of a variety of malignancies, including leukemia and cancers of the lung and prostate.[1,2] Knowledge of the specific biological pathways perturbed by nontoxic concentrations of Cd^{2+} may give rise to improved risk assessment and the development of preventive and therapeutic strategies for Cd^{2+} exposure. Most of our current understanding about the mechanisms of Cd^{2+} carcinogenesis and toxicity is derived from experiments conducted with the use of a wide variety of in vitro cell culture and in vivo animal models.[2,4] These studies revealed various modes of action for Cd^{2+} toxicity. These include modulation of gene expression and signal transduction, generation of reactive oxygen species (ROS), interference with cellular antioxidant defense enzymes, inhibition of DNA repair, disruption of E-cadherin-mediated cell−cell adhesion, and interference with the functions of essential metals.[1,2,5] Nevertheless, the potential interactions and relative contributions of these various mechanisms to overall Cd^{2+} toxicity are not well-established.

We reason that a more complete understanding about the overall mechanism of Cd^{2+} toxicity requires the assessment about how cells respond to Cd^{2+} exposure as a whole. In many cases, organisms attempt to adapt to environmental toxicants by modulating the expression of specific genes and proteins. Therefore, identifying those proteins that are up or down-regulated upon exposure to a specific toxic agent may provide insights into the mechanisms of action for the toxicant. Mass

Received: November 23, 2013
Published: February 14, 2014

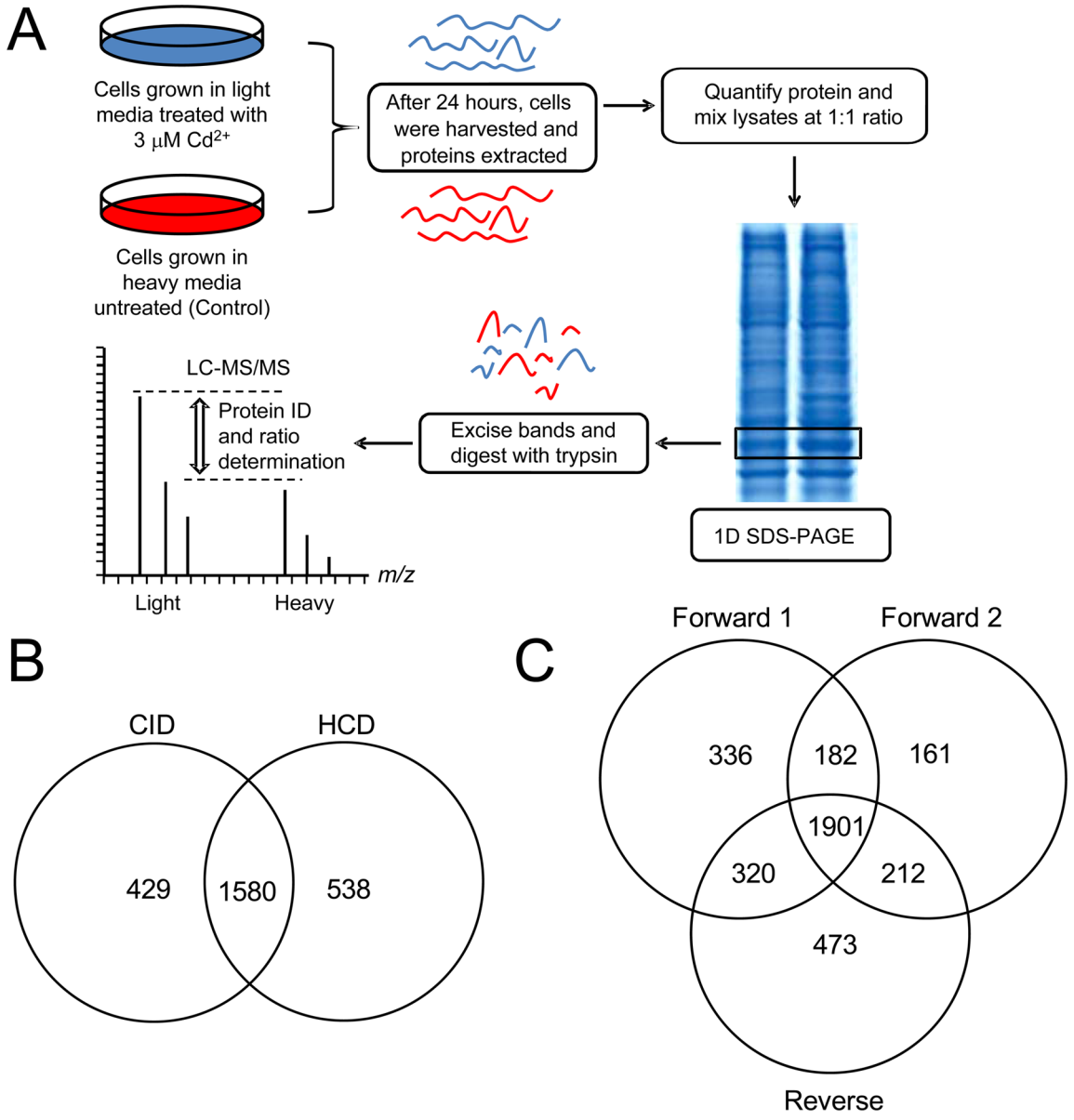

Figure 1. SILAC-based quantitative proteomics. (A) Flowchart of forward SILAC coupled with LC−MS/MS for the comparative analysis of protein expression in GM00637 cells following Cd^{2+} treatment. In forward SILAC experiments, light Lys- and Arg-labeled cells were treated with 3 μM Cd^{2+}, whereas the heavy Lys- and Arg-labeled cells were used as the control. (B) Venn diagram summarizing the improved protein identification and quantification achieved by combining HCD and CID fragmentation techniques. (C) Venn diagram summarizing the number of proteins quantified from three independent SILAC (two forward and one reverse) experiments.

spectrometry-based quantitative proteomics has emerged as a powerful tool for environmental toxicology studies because this technique can be used to assess the relative changes in expression for thousands of proteins in a single experiment.[6] Several studies have been carried out to exploit the Cd^{2+}-induced alteration of the global proteome in the leaf and root of plants[7−9] as well as various tissues of fish and other aquatic species.[10−13] The results from these studies support that many proteins involved in antioxidant defense response, glutathione metabolism, and cellular energy production were upregulated in response to Cd^{2+} exposure.[10−13] A few studies have also been conducted to examine the Cd^{2+}-induced perturbation of proteins in mammalian cells;[14,15] however, very modest numbers of proteins were quantified in these studies, which hampers a systematic interrogation of the cellular pathways altered by exposure to the toxic metal ion.

In this study, we employed a quantitative proteomic technique, which is based on stable isotope labeling by amino acids in cell culture (SILAC) and LC−MS/MS, to assess the perturbation of protein expression in GM00637 human skin fibroblast cells following Cd^{2+} exposure. Our proteomic analysis allowed for the identification and quantification of ∼3000 proteins in GM00637 human skin fibroblast cells. Among them, ∼1900 were quantified in all three independent SILAC-labeling experiments, and 400 demonstrated significantly altered expression upon Cd^{2+} exposure. In agreement with previous findings, our proteomic analysis demonstrated the significant upregulation of proteins involved in antioxidant defense, glutathione biosynthesis and homeostasis, cellular energy metabolism, and adherens junctions. Furthermore, we found that Cd^{2+} treatment induced the upregulation of two isoforms of dimethylarginine dimethylaminohydrolase (DDAH I and II),

dx.doi.org/10.1021/pr401159f | J. Proteome Res. 2014, 13, 1677−1687

which stimulated NO biosynthesis in human lung and skin fibroblast cells.

MATERIALS AND METHODS

Materials

Heavy lysine and arginine ($[^{13}C_6,^{15}N_2]$-L-lysine and $[^{13}C_6]$-L-arginine) were purchased from Cambridge Isotope Laboratories (Andover, MA). Cadmium chloride ($CdCl_2$) and all other chemicals/reagents, unless otherwise stated, were purchased from Sigma-Aldrich (St. Louis, MO).

Cell Culture

GM00637 human skin fibroblast cells (kindly provided by Prof. Gerd P. Pfeifer, City of Hope, Duarte, CA) and IMR-90 human lung fibroblast cells (ATCC, Manassas, VA) were cultured in Iscove's modified Dulbecco's medium (IMDM) and Eagle's minimum essential medium (EMEM), respectively. The culture media were supplemented with 10% fetal bovine serum (FBS, Invitrogen, Carlsbad, CA) and penicillin/streptomycin (100 IU/mL). Cells were maintained in a humidified atmosphere with 5% CO_2 at 37 °C, and the culture medium was changed in every 2 to 3 days as necessary.

The complete light- and heavy-IMDM media for SILAC experiments were prepared by the addition of light or heavy lysine and arginine along with 10% dialyzed FBS to the lysine- and arginine-depleted IMDM medium that was custom-prepared following ATCC formulation. The GM00637 cells were cultured in the heavy-IMDM medium for at least 10 days or 5 cell doublings to achieve complete heavy-isotope incorporation. GM00637 cells were cultured to a density of approximately 7.5×10^5 cells/mL. The cells were washed twice with ice-cold phosphate-buffered saline (PBS) to remove the residual FBS, and the media was replaced with FBS-free heavy or light media containing 3 μM Cd^{2+} or vehicle control (Millipore H_2O). To ensure that the observed changes in protein-expression ratio are not due to incomplete heavy-isotope incorporation, we performed both forward and reverse SILAC-labeling experiments. In forward SILAC experiments, the cells cultured in light medium were treated with 3 μM Cd^{2+} for 24 h, whereas the cells cultured in heavy medium were untreated and used as control (Figure 1A). In reverse SILAC experiments, cells cultured in the heavy medium were treated with Cd^{2+}, and light cells were used as the untreated control. After 24 h, the light and heavy cells were collected by centrifugation at 3000*g* at 4 °C and washed three times with ice-cold PBS. The cell pellets were resuspended in the CelLytic M cell lysis buffer containing a protease inhibitor cocktail (Sigma-Aldrich) and placed on ice for 30 min with vortexing at 10 min intervals. Cell lysates were centrifuged at 12 000*g* at 4 °C for 30 min, and the resulting supernatants were collected. The protein concentrations of the cell lysates were determined by using Quick Start Bradford protein assay kit (Bio-Rad, Hercules, CA). In forward and reverse SILAC experiments, the light and heavy lysates of Cd^{2+}-treated cells were mixed with the heavy and light lysates from untreated cells, respectively, at a 1:1 ratio (by mass), reduced with dithiothreitol, alkylated with iodoacetamide, and digested with trypsin at an enzyme/protein ratio of 1:100.

LC–MS/MS for Protein Identification and Quantification

Peptide samples were automatically injected and separated by online liquid chromatography on an EASY-nLC II and analyzed on an LTQ Orbitrap Velos mass spectrometer equipped with a nanoelectrospray ionization source (Thermo, San Jose, CA), as described previously.[16] A homemade trapping column (150 μm × 50 mm) and a separation column (75 μm × 120 mm), packed with ReproSil-Pur C18-AQ resin (3 μm in particle size, Dr. Maisch HPLC GmbH, Germany), were employed for the separation of peptide mixtures. Peptide samples were initially loaded onto the trapping column with a solvent mixture of 0.1% formic acid in CH_3CN/H_2O (2:98, v/v) at a flow rate of 4.0 μL/min. The peptides were then separated using a 120 min linear gradient of 2–40% acetonitrile in 0.1% formic acid, and the flow rate was 300 nL/min. The LTQ-Orbitrap Velos mass spectrometer was operated in the positive-ion mode, and the spray voltage was 1.8 kV. The data were acquired in data-dependent scan mode where one full-scan MS was followed with 20 MS/MS scans. The full-scan mass spectra (m/z 350–2000) were recorded with a resolution of 60 000 at m/z 400 after accumulation to a target value of 5×10^5. The 20 most abundant ions found in MS at a threshold above 500 counts were selected for fragmentation by higher-energy collision-induced dissociation (HCD) or collisionally induced dissociation (CID) at a normalized collision energy of 35% (Figure 1B).

Data Processing

Database search was conducted in MaxQuant (version B.01.03) against the human International Protein Index version 3.68 (87 083 entries) to which contaminants and reverse sequences were added.[17] The search was performed with mass tolerances of 25 ppm for precursor ions and 0.6 Da for fragment ions. We included cysteine carbamidomethylation and methionine oxidation as fixed and variable modifications, respectively. SILAC-quantification setting was adjusted to doublets, with lysine (+8 Da) and arginine (+6 Da) being selected as heavy labels. Only proteins with at least two peptides being identified by MS/MS were considered reliably identified. The minimal peptide length was six amino acids, and the maximum number of miss-cleavage events for trypsin was set at two per peptide. For peptide and protein identification, the false discovery rates were set at 1% at both the peptide and protein levels.[17] The quantification was based on three independent SILAC and LC–MS/MS experiments, which included two forward and one reverse SILAC labelings, and the significantly changed proteins discussed later could be quantified in all three sets of SILAC experiments (Figure 1C).

Biological Pathways and Protein Interaction Network Analysis

Proteins with significant changes (>1.5- or <0.67-fold) in expression following Cd^{2+} treatment were further analyzed using DAVID,[18] which revealed the Cd^{2+}-induced perturbation of multiple cellular pathways in GM00637 cells (Table S3). Pathways with p values less than 0.05 were considered significant. To assess the interactions among the cellular pathways identified from the DAVID analysis, the proteins identified for each pathway were subjected to protein interaction network analysis using the STRING tool (version 9.05, http://string.embl.de/), which predicts protein–protein associations based on literature data and databases of archived biological pathway knowledge.[19]

Nitric Oxide Measurement

Nitric oxide production was assessed by measuring the total nitrate/nitrite concentrations in cell lysates and cell culture media following Cd^{2+} treatment with the use of a colorimetric

dx.doi.org/10.1021/pr401159f | J. Proteome Res. 2014, 13, 1677–1687

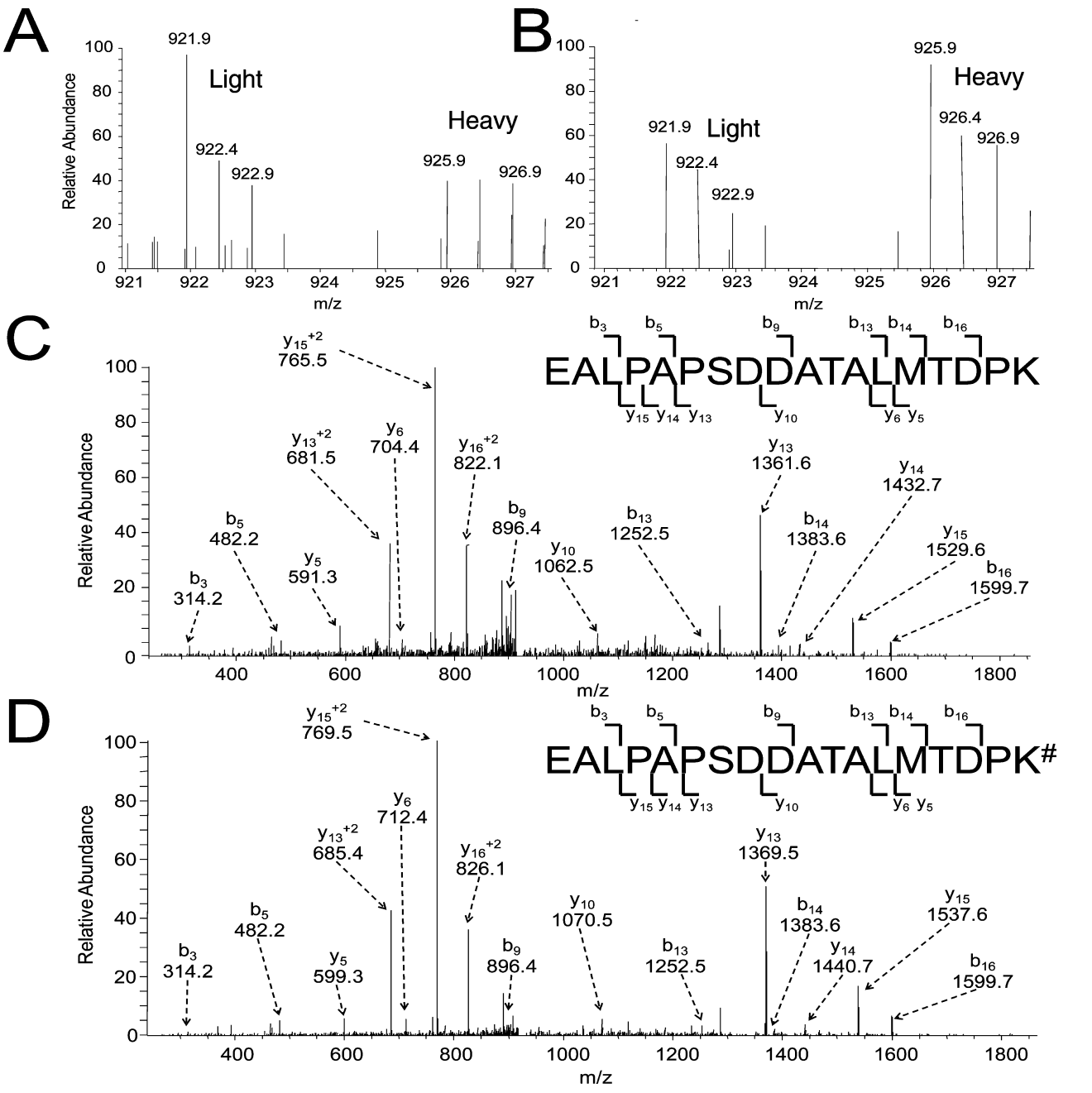

Figure 2. Representative LC–MS/MS data revealed the Cd^{2+}-induced upregulation of the peptide EALPAPSDDATALMTDPK from glutathione peroxidase 1. Shown are the isotopic peaks for the $[M + 2H]^{2+}$ ions of the light- (Light) and heavy (Heavy) lysine-bearing peptide EALPAPSDDATALMTDPK from forward (A) and reverse (B) SILAC samples. The intensity of the monoisotopic peaks was employed for calculating the protein-expression ratio. The sequence for both the light- and heavy-lysine labeled peptide was confirmed by MS/MS analysis (C, D).

assay kit (BioVision Inc., Milpitas, CA). The standard assay protocol included with the kit was followed with minor modifications. Briefly, cells were treated with 3 μM Cd^{2+} or vehicle control for 0, 6, 12, or 24 h. At each time point, the cell culture medium was collected for nitrate/nitrite measurements, and the cells were subsequently washed with ice-cold PBS and harvested by centrifugation at 4000*g* for 10 min. The cell pellet was subsequently homogenized in the assay sample buffer included with the kit. Cell culture media and cell pellet samples were further diluted, as necessary, and nitrate reductase mixture and enzyme cofactor (included with the kit) were added to each sample well and allowed to incubate at room temperature for 1 h to convert nitrate to nitrite. Following the incubation, Griess Reagent was added to each well, and color development took place at room temperature for 10 min. Absorbance was read at 540 nm using a microtiter plate reader (Wallac 1420 VICTOR2, PerkinElmer Inc., Waltham, MA).

Western Blot

GM00637 and IMR-90 cells were cultured in T25 cell culture flasks until ~80% confluence was reached, as described above. The cells were washed twice with ice-cold PBS to remove the residual FBS, and the media was replaced with FBS-free culture media containing 3 μM Cd^{2+}. The protein concentrations of the cell lysates were determined by using Quick Start Bradford protein assay kit (Bio-Rad, Hercules, CA), and 30 μg of

dx.doi.org/10.1021/pr401159f | J. Proteome Res. 2014, 13, 1677–1687

Table 1. Pathways That Are Significantly Altered in GM00637 Cells following a 24 h Exposure to 3 μM Cd^{2+}[a]

International Protein Index	UniProt ID	protein name	average ratio (treated/untreated)
(A) Nitric Oxide Synthesis			
IPI00220342	DDAH1	dimethylarginine dimethylaminohydrolase 1	1.52 ± 0.11
IPI00000760	DDAH2	dimethylarginine dimethylaminohydrolase 2	1.64 ± 0.26
(B) Antioxidant Enzymes			
IPI00008752	MT1G	metallothionein-1G	5.44 ± 4.74
IPI00219025	GLRX1	glutaredoxin-1	2.10 ± 0.99
IPI00008552	GLRX3	glutaredoxin-3	1.86 ± 0.95
IPI00218733	SODC	superoxide dismutase [Cu−Zn]	1.55 ± 0.26
IPI00646689	TXD17	14 kDa thioredoxin-related protein	1.50 ± 0.16
(C) Glutathione Metabolism			
IPI00031564	GGCT	gamma-glutamyl cyclotransferase	1.69 ± 0.38
IPI00246975	GSTT1	glutathione S-transferase mu 3	2.00 ± 0.33
IPI00019755	GSTP1	glutathione S-transferase omega 1	1.93 ± 0.68
IPI00219757	Q6FGJ9	glutathione *S*-transferase pi 1	1.55 ± 0.24
IPI00741097	GSTO1	glutathione S-transferase theta 1	1.78 ± 0.31
IPI00556579	MAAI	glutathione S-transferase zeta 1	1.66 ± 0.44
IPI00016862	Q9UQS1	glutathione reductase	1.67 ± 0.10
IPI00010706	Q6FHQ6	glutathione synthetase	1.54 ± 0.20
IPI00027223	Q03504	isocitrate dehydrogenase 1 (NADP+)	1.61 ± 0.23
IPI00005102	Q6NSD4	spermine synthase	1.84 ± 0.20
IPI00927606	Q8TDA8	glutathione peroxidase	1.56 ± 0.12
(D) Glycolysis and Gluconeogenesis			
IPI00169383	PGK1	phosphoglycerate kinase 1	1.69 ± 0.05
IPI00479186	Q9NYI7	pyruvate kinase M2	1.56 ± 0.39
IPI00465028	Q53HE2	triosephosphate isomerase	1.58 ± 0.35
IPI00418262	ALDOC	fructose-bisphosphate aldolase C	1.56 ± 0.23
IPI00549725	Q6P6D7	BPG-dependent PGAM 1	1.53 ± 0.23
IPI00479877	AK1A1	aldehyde dehydrogenase E3 isozyme	1.59 ± 0.17
IPI00220271	AL9A1	aldehyde reductase	1.54 ± 0.22
IPI00332371	Q6MZK4	phosphofructo-1-kinase isozyme B	1.50 ± 0.25
IPI00947127	A8MXQ4	L-lactate dehydrogenase	1.58 ± 0.15
IPI00219217	Q5U077	L-lactate dehydrogenase B chain	1.62 ± 0.33
IPI00796333	ALDOA	fructose-bisphosphate aldolase A	1.62 ± 0.21
IPI00216171	Q6FHV6	enolase 2	1.59 ± 0.24
IPI00219018	Q16768	glyceraldehyde-3-phosphate dehydrogenase	1.68 ± 0.47
IPI00027497	Q59F85	glucose-6-phosphate isomerase	1.51 ± 0.29
IPI00941899	Q9NYI7	pyruvate kinase 2/3	1.54 ± 0.28
IPI00015911	DLDH	dihydrolipoamide dehydrogenase	1.67 ± 0.18
IPI00465248	Q96GV1	alpha-enolase	1.55 ± 0.35
(E) Pentose Phosphate Pathway			
IPI00219616	Q15244	phosphoribosyl pyrophosphate synthase I	1.50 ± 0.16
IPI00029997	6PGL	6-phosphogluconolactonase	1.56 ± 0.28
IPI00418262	ALDOC	fructose-bisphosphate aldolase C	1.56 ± 0.23
IPI00796333	ALDOA	fructose-bisphosphate aldolase A	1.62 ± 0.21
IPI00335280	Q53TV9	ribulose-5-phosphate-3-epimerase	1.55 ± 0.06
IPI00332371	Q6MZK4	phosphofructo-1-kinase isozyme B	1.50 ± 0.25
IPI00027497	Q59F85	glucose-6-phosphate isomerase	1.51 ± 0.29
(F) Pyruvate Metabolism			
IPI00479186	Q9NYI7	pyruvate kinase M2	1.56 ± 0.39
IPI00413641	ALDR	aldehyde reductase	1.55 ± 0.20
IPI00003933	GLO2	hydroxyacylglutathione hydrolase, mitochondrial	1.50 ± 0.17
IPI00008215	Q8WVX2	malic enzyme 1	1.71 ± 0.35
IPI00396015	AL9A1	acetyl-CoA carboxylase 1	0.54 ± 0.18
IPI00479877	ACACA	aldehyde dehydrogenase E3 isozyme	1.59 ± 0.17
IPI00291419	Q59GW6	acetyl-CoA acetyltransferase, cytosolic	1.63 ± 0.11
IPI00947127	A8MXQ4	L-lactate dehydrogenase	1.58 ± 0.15
IPI00941899	Q9NYI7	pyruvate kinase 2/3	1.54 ± 0.28
IPI00015911	DLDH	dihydrolipoamide dehydrogenase	1.67 ± 0.18
IPI00219217	Q5U077	L-lactate dehydrogenase B chain	1.62 ± 0.33
IPI00030363	Q96FG8	ccetoacetyl-CoA thiolase	1.56 ± 0.09

dx.doi.org/10.1021/pr401159f | *J. Proteome Res.* 2014, 13, 1677−1687

Table 1. continued

International Protein Index	UniProt ID	protein name	average ratio (treated/untreated)
(G) The Citric Acid Cycle			
IPI00025366	Q0QEL2	citrate synthase, mitochondrial	1.60 ± 0.19
IPI00096066	Q9Y436	GTP-specific succinyl-CoA synthetase subunit beta	1.53 ± 0.10
IPI00464979	Q5T9Q5	ATP-specific succinyl-CoA synthetase subunit beta	1.63 ± 0.36
IPI00027223	Q6FHQ6	cytosolic NADP-isocitrate dehydrogenase	1.61 ± 0.23
IPI00304417	Q9NUZ0	isocitrate dehydrogenase [NAD] subunit beta, mitochondrial	1.85 ± 0.03
IPI00872762	SUCA	succinyl-CoA ligase [GDP-forming] subunit alpha, mitochondrial	1.50 ± 0.07
IPI00015911	DLDH	dihydrolipoamide dehydrogenase	1.67 ± 0.18
(H) Adherens Junction			
IPI00385055	CTNA2	alpha N-catenin	0.40 ± 0.41
IPI00009342	Q05DN7	Ras GTPase-activating-like protein IQGAP1	1.65 ± 1.17
IPI00003479	Q499G7	extracellular signal-regulated kinase 2	1.55 ± 0.15
IPI00018195	Q8NHX1	extracellular signal-regulated kinase 1	1.73 ± 0.33
IPI00215948	CTNA1	alpha E-catenin	0.67 ± 0.14
IPI00409590	Q5TBK5	F-box only protein 20	2.94 ± 2.39
IPI00021440	Q562Y8	actin, cytoplasmic 2	1.51 ± 0.00
IPI00013808	ACTN4	alpha-actinin-4	1.51 ± 0.24
IPI00942869	Q96FS1	cadherin-associated Src substrate	1.74 ± 1.56

[a]Also shown are the list of proteins associated with each of these pathways that are quantified in the present study.

protein/sample was used for immunoblotting of DDAH I. Proteins were separated by SDS-PAGE and transferred to nitrocellulose membranes for immunoblotting. Briefly, proteins were suspended in an equal volume of Laemmli buffer, heated at 95 °C for 5 min, and loaded and separated on 12% SDS-PAGE with a 4% stacking gel. Proteins were subsequently transferred to nitrocellulose membrane and blocked in 5% milk in PBS-T buffer (1× PBS, 0.1% Tween 20, and 5% dry milk). Membranes were washed in PBS-T and incubated overnight at 4 °C with DDAH I primary antibody (ab2231, Abcam, Cambridge, MA, 1:1000 dilution). Membranes were then washed in PBS-T, incubated with HRP-conjugated anti-goat secondary antibody (sc-2020, Santa Cruz Biotechnology, Dallas, TX, 1:2000 dilution) for 2 h, and washed in PBS-T before imaging with a Typhoon 9410 variable mode imager (GE Healthcare Biosciences, Pittsburgh, PA). Membranes were reprobed with anti-actin antibody (ab8227, Abcam, Cambridge, MA, 1:10 000 dilution) to confirm equal protein loading. Band pixel intensity was measured using ImageQuant (GE Healthcare Biosciences). Band intensities for DDAH I from control and Cd^{2+}-treated groups were normalized to that of actin.

RNA Extraction and Quantitative Real-Time PCR Analysis

Total RNA was extracted using the RNeasy Mini Kit (Qiagen, Valencia, CA) and reverse transcribed by employing M-MLV reverse transcriptase (Promega, Madison, WI) and a poly(dT) primer. Quantitative real-time PCR was performed with iQ SYBR green supermix kit (Bio-Rad, Hercules, CA) on a Bio-Rad MyiQ thermal cycler, and gene-specific primers are listed in Supporting Information Table S5. The comparative cycle threshold method was utilized for the relative quantification of gene-expression level, and *GAPDH* gene was used as the internal control. The mRNA level of each gene was normalized to that of the internal control.[20]

RESULTS AND DISCUSSION

Protein Identification and Quantification

To exploit the comprehensive mechanisms of Cd^{2+} toxicity, we assessed the Cd^{2+}-induced perturbation of protein expression in GM00637 human skin fibroblast cells by employing a quantitative proteomic strategy relying on SILAC-based metabolic labeling and LC−MS/MS analysis. The skin fibroblast cells were chosen because dermal contact constitutes a major route of human exposure to cadmium.[1,2] Toward this end, we treated the GM00637 cells with 3 μM Cd^{2+} for 24 h, which was found to induce a less than 5% cell death, as determined by trypan blue-exclusion assay (Figure S1). It is of note that we employed serum-free media for all Cd^{2+}-treatment experiments to prevent the potential interactions between Cd^{2+} and proteins in the FBS. To ensure that the observed changes in protein expression arose from Cd^{2+} treatment, we conducted the SILAC experiments in three biological replicates, including both forward and reverse SILAC labeling (Figure 1 and Materials and Methods). Figure 2A,B displays the ESI−MS results of the tryptic peptide EALPAPSDDATALMTDPK from glutathione peroxidase 1, which supports unequivocally the Cd^{2+}-induced upregulation of this protein in both forward and reverse SILAC experiments. The MS/MS results also supported the sequence for the light- and heavy-labeled peptide (Figure 2C,D).

The LC−MS/MS results for the three sets of SILAC samples led to the identification and quantification of 3257 and 2931 proteins, respectively. A total of 1901 proteins could be quantified in both forward and reverse SILAC-labeling experiments (Figure 1C; the detailed quantification results for these proteins are summarized in Table S1). The majority of the quantified proteins were not altered by Cd^{2+} treatment, with an average ratio and mean relative standard deviation of ratios for all quantified proteins being ∼1.0 and 20%, respectively. Thus, we selected a ratio of >1.5 or <0.67 as threshold for screening the significantly changed proteins.[21,22] Among the quantified proteins, 400 displayed significant changes upon Cd^{2+} treatment, with 88 and 312 being down- and upregulated, respectively (Table S2).

Protein Pathway and Network Analysis

Proteins with significant changes in expression following Cd^{2+} treatment were further subjected to bioinformatic analysis using DAVID, which unveiled the perturbation of multiple cellular KEGG pathways in GM00637 cells (Table S3). These included glutathione metabolism, glycolysis and gluconeogenesis,

dx.doi.org/10.1021/pr401159f | J. Proteome Res. 2014, 13, 1677−1687

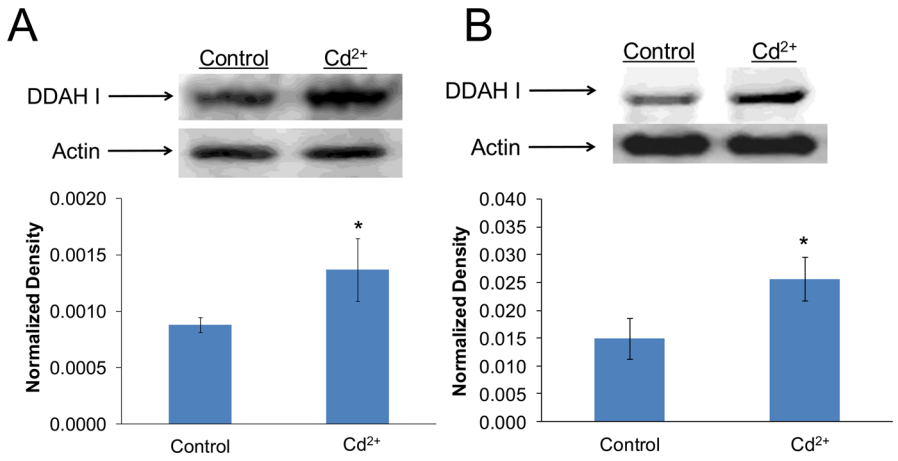

Figure 3. Western blot analysis for DDAH I in human skin (GM00637; A) and lung (IMR90; B) fibroblast cells following a 24 h exposure to 3 μM Cd^{2+}. Data represent the mean ± standard deviation (n = 3). *, $p < 0.05$, student's t test.

pyruvate metabolism, pentose phosphate pathway, fatty acid metabolism, and the citric acid cycle (Table S3). To assess the interactions among the various cellular pathways identified from the DAVID analysis, we subjected the proteins identified for each pathway to protein interaction network analysis using the STRING tool (Materials and Methods). The results from the STRING analysis for the aforementioned pathways are summarized in Table S4.

Cd^{2+} Treatment Led to Overexpression of DDAH I and II and Elevated Production of NO (Table 1)

The ability of Cd^{2+} to induce oxidative stress through the generation of ROS and reactive nitrogen species (RNS) is well-established and has been implicated in Cd^{2+} toxicity.[2,5] A previous study suggested that Cd^{2+} could inhibit NO production in endothelial cells,[23] whereas other studies demonstrated the ability of Cd^{2+} to induce NO formation in macrophages.[24,25] The results from our quantitative proteomic analysis revealed that Cd^{2+} treatment induced the upregulation of DDAH I and II (by 1.52- and 1.64-fold, respectively, Table 1), two enzymes that are important in NO biogenesis.[26] Western blot analysis further validated the upregulation of DDAH I in human skin (GM00637 cells) and lung (IMR-90 cells) fibroblast cells (Figure 3).

DDAH is responsible for the degradation of asymmetric dimethylarginine, an endogenous inhibitor of NO synthase.[26] The upregulation of DDAH I and II suggests that Cd^{2+} treatment may result in elevated NO production in GM00637 cells. To test this, we measured the total nitrate/nitrite concentrations using a NO colorimetric assay (Materials and Methods). Our results showed that the total nitrite/nitrate levels were significantly increased in both the lysates and the culture media of GM00637 (Figure 4) and IMR90 (Figure S3) cells following a 12 h exposure to 3 μM Cd^{2+}. Although elevated NO formation was previously observed in macrophages following Cd^{2+} exposure,[24,25] our data supported that Cd^{2+} exposure also led to an increase in NO biosynthesis in human skin and lung fibroblasts. Furthermore, our results indicate that the increase in NO production following Cd^{2+} exposure may involve the upregulation of DDAH I and II.

Antioxidant Enzymes and Glutathione Metabolism

We found that Cd^{2+} exposure induced a significant upregulation of several important antioxidant enzymes including superoxide dismutase, metallothionein 1-G, glutaredoxin 1, and glutaredoxin 3, whose expression levels were elevated by 1.55-, 5.44-, 2.10-, and 1.86-fold, respectively (Table 1). These results are in keeping with the previous findings that exposure to Cd^{2+} could activate antioxidant defense systems consisting of enzymes and metabolites protecting organisms from oxidative damage.[2,5] Our finding is also in line with results from a previous quantitative proteomic study showing that the exposure to Cd^{2+} led to elevated expression of metallothionein and phytochelatins in *Arabidopsis* roots.[7]

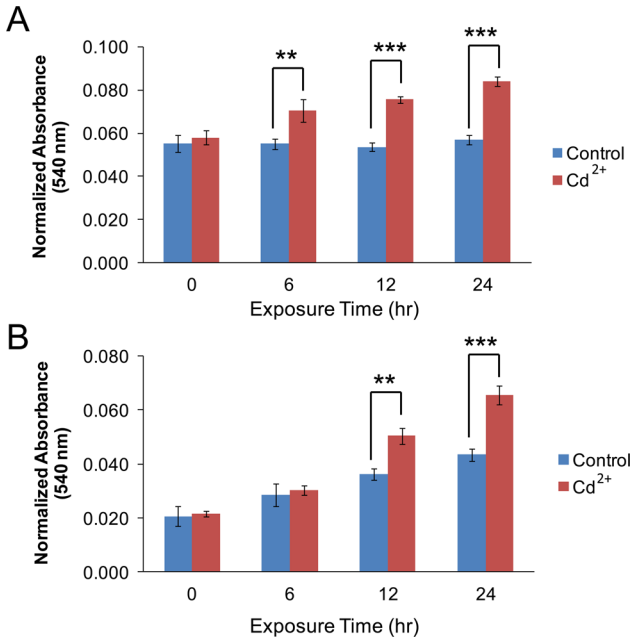

Figure 4. Cd^{2+} treatment led to alterations in total nitrate/nitrite concentrations in GM00637 human skin fibroblast cells. The GM00637 cells were treated with 3 μM Cd^{2+} for 24 h, and total nitrate/nitrite concentrations were measured in cell lysates (A) and cell culture media (B). The data represent the mean ± standard deviation (n = 3). **, $p < 0.01$; ***, $p < 0.001$, student's t test.

Apart from the upregulation of antioxidant enzymes, Cd^{2+} treatment induced markedly elevated expression of proteins involved in GSH metabolism. The ability of nontoxic concentrations of Cd^{2+} to induce elevated levels of GSH has been documented, where GSH is thought to bind to Cd^{2+} ions and to be the major antioxidant for counteracting Cd^{2+}-induced

dx.doi.org/10.1021/pr401159f | J. Proteome Res. 2014, 13, 1677−1687

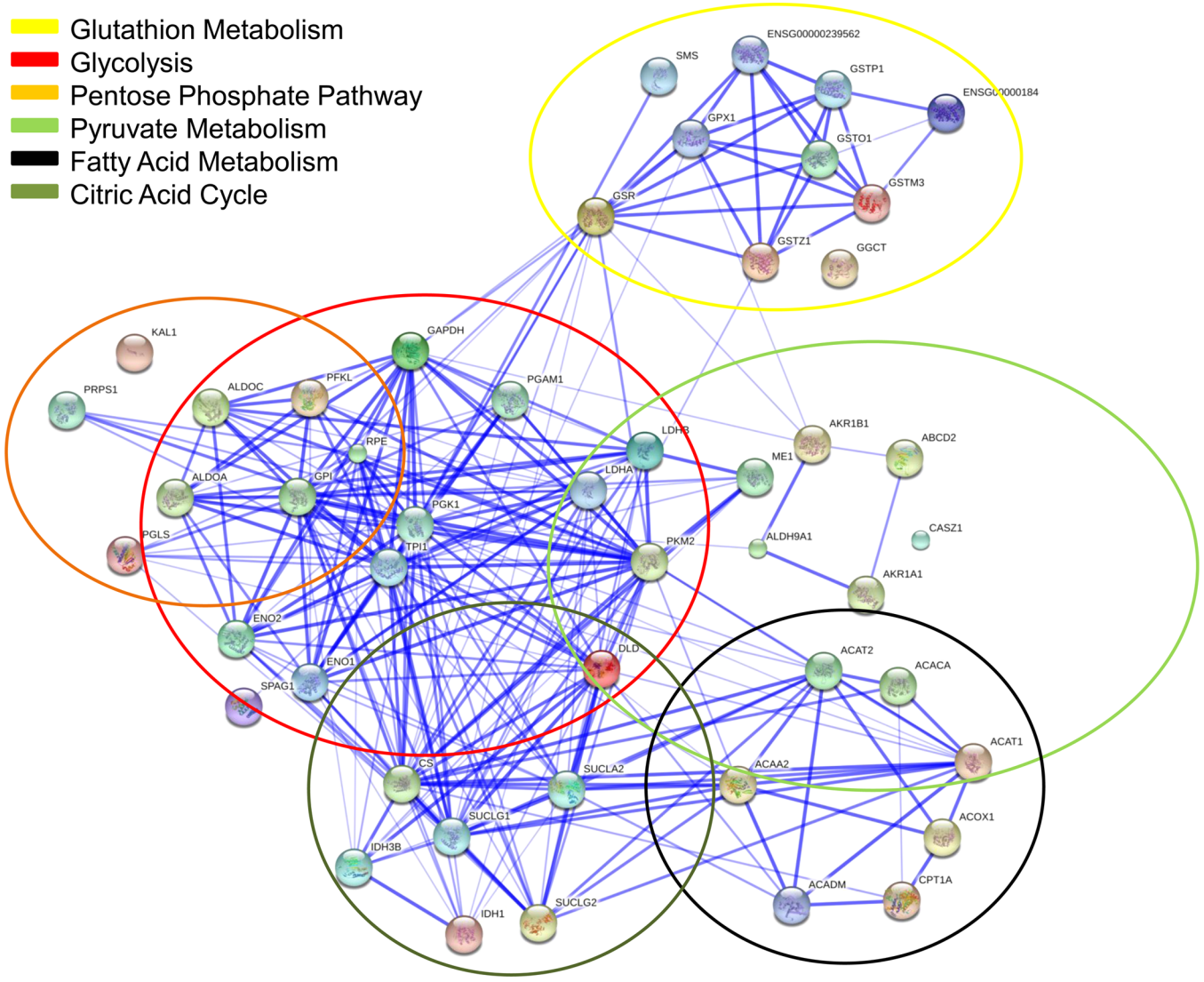

Figure 5. Biological pathways and protein interaction network analysis. Primary KEGG pathways altered upon Cd^{2+} exposure were identified by bioinformatic analysis using DAVID. Proteins with >1.5- or <0.67-fold change in expression following Cd^{2+} treatment were included for the analysis, and KEGG pathways with p values less than 0.05 were considered significant (Table S3). STRING tool was used for protein interaction network analysis.

oxidative stress.[1,5] In agreement with these previous findings, we observed the Cd^{2+}-induced upregulation of five different isoforms of GSH S-transferases (GSTs), GST pi 1, GST mu 3, GST theta 1, GST zeta 1, and GST omega 1, by 1.55-, 2.00-, 1.78-, 1.66-, and 1.93-fold, respectively (Table 1). GSTs play primary roles in the detoxification of various xenobiotics through GSH conjugation.[27] In addition to the GSTs, several other important proteins involved in glutathione metabolism, glutathione reductase, glutathione peroxidase, and glutathione synthase, were increased by 1.67-, 1.56-, and 1.54-fold, respectively, following Cd^{2+} treatment (Table 1).

Cellular Energy Metabolism

Our proteomic analysis also uncovered a substantial upregulation of several pathways that are crucial in cellular energy metabolism, including glycolysis and gluconeogenesis, pyruvate metabolism, and the citric acid cycle. Glycolysis is a metabolic process converting glucose into pyruvate to produce ATP and NADH.[28] The pentose phosphate pathway is an alternative process of glycolysis, and it results in the generation of NADPH, which is employed by glutathione reductase to reduce glutathione;[29] the reduced glutathione is then used by glutathione peroxidase to detoxify lipid hydroperoxides and H_2O_2, thereby diminishing oxidative stress.[30] Our quantitative proteomic experiments revealed the upregulation of 17 and 7 proteins in the glycolysis and pentose phosphate pathways, respectively, in GM00637 cells following Cd^{2+} exposure (Table 1).

Pyruvate resides at an intersection of several key pathways of energy metabolism, where it is the end product of glycolysis and the starting point for gluconeogenesis. Pyruvate can be converted to acetyl-CoA for use in the citric acid cycle or serve as the starting point for cholesterol and fatty acid biosynthesis.[28,31] Our proteomic analysis revealed that Cd^{2+} exposure of human skin fibroblast cells led to altered expression of 12 proteins associated with pyruvate metabolism (Table 1). All of them except acetyl-CoA carboxylase 1, whose expression was reduced by ~2-fold, were upregulated following Cd^{2+} treatment. The Cd^{2+}-induced decline of acetyl-CoA carboxylase may block the use of acetyl-CoA for fatty acid biosynthesis. We also

dx.doi.org/10.1021/pr401159f | J. Proteome Res. 2014, 13, 1677−1687

employed RT-PCR to monitor the mRNA levels of two genes encoding important enzymes associated with cholesterol biosynthesis, namely, 3-hydroxy-3-methylglutaryl-CoA reductase (*HMGCR*) and farnesyl diphosphate synthase (*FDPS*),[32] following Cd^{2+} exposure. Our results showed significant reductions in mRNA levels of *HMGCR* and *FDPS* (Figure S2), suggesting that Cd^{2+} exposure may also result in diminished cholesterol biosynthesis. The citric acid cycle, a.k.a. the tricarboxylic acid cycle (TCA cycle), is utilized by aerobic organisms to produce ATP through the oxidization of acetate derived from carbohydrates, fatty acids, and proteins.[33] Here, we found that seven proteins involved in the TCA cycle were significantly elevated in response to Cd^{2+} treatment. These included citrate synthase, GTP-specific succinyl-CoA synthetase subunit beta, ATP-specific succinyl-CoA synthetase subunit beta, cytosolic NADP-isocitrate dehydrogenase, isocitrate dehydrogenase [NAD] subunit beta, succinyl-CoA ligase [GDP-forming] subunit alpha, and dihydrolipoamide dehydrogenase, which were upregulated by 1.60-, 1.53-, 1.63-, 1.61-, 1.85-, 1.50-, and 1.67-fold, respectively (Table 1). These results together indicate that Cd^{2+} treatment led to diversion of acetyl-CoA toward the citric acid cycle, thereby meeting the cellular energy demand.

Our findings made from quantitative proteomic experiments are in line with previous studies showing that Cd^{2+} exposure confers increased cellular energy metabolism. In this vein, a recent study by Faiz et al.[34] demonstrated that exposure to $CdCl_2$ resulted in a dose-dependent reduction of cellular levels of glucose, ATP, and acetyl-coenzyme A. A previous proteomic experiment also showed that exposure to Cd^{2+} could result in elevated levels of expression of proteins involved in glycolysis and citric acid cycle in poplar leaves.[9] Likewise, the activities of enzymes in the citric acid cycle were found to be significantly increased in tomato roots upon exposure to Cd^{2+}.[35] In addition, upregulation of photosynthesis-related proteins was found in *Arabidopsis* shoots following Cd^{2+} exposure, suggesting that the accumulation of Cd^{2+} in shoots elicits a greater energy demand.[8] These previous studies, together with the present investigation, support that the Cd^{2+}-induced elevation in cellular energy metabolism is conserved among species.

Adherens Junction

Another interesting finding made from the DAVID bioinformatic analysis was the perturbation of the adherens junction pathway. Cd^{2+} is thought to interact directly with E-cadherin and disrupt cell−cell adhesion.[4] In addition, Prozialeck et al.[36] found that Cd^{2+} can deregulate cell proliferation through the disruption of the cadherin-mediated cell−cell adhesion in kidney epithelial cells. In line with these previous findings, our proteomic data revealed that the expression levels for nine proteins associated with adherens junction were significantly altered in response to Cd^{2+} exposure (Table 1).

■ CONCLUSIONS

Over the last several decades, a great deal of data have been obtained on Cd^{2+} toxicology, which make it increasingly clear that the toxic effects of Cd^{2+} on biological systems are diverse and elicited through a complex array of mechanisms. Along this line, Cd^{2+} was found to exert a wide variety of cellular effects, including the ability to induce oxidative stress,[4,5] thereby interfering with the normal physiological functions of cells and ultimately leading to a number of human diseases, including cancer.[2,4] Despite the large number of studies aimed at elucidating the toxic effects of Cd^{2+}, few have been directed toward investigating Cd^{2+}'s ability to disrupt multiple cellular pathways simultaneously and the overall cellular responses toward Cd^{2+} exposure, particularly for mammalian cells. In this study, our unbiased proteomic analysis provided an unprecedented coverage of the proteome that was altered in response to Cd^{2+} exposure, which demonstrated that Cd^{2+} exposure results in the concomitant alterations of multiple cellular pathways in human fibroblast cells. These pathways together paint a more comprehensive and complete picture of the initial cellular responses to Cd^{2+} exposure. Indeed, DAVID and STRING analyses demonstrated that many of the pathways identified in our proteomic analysis interact, directly or indirectly, with each other (Figure 5), lending further evidence that support the synergistic effects from the perturbation of multiple cellular pathways contributing to the overall effects of Cd^{2+} on biological systems.

The induction of ROS and the ensuing generation of oxidative stress are thought to be the central pillars in Cd^{2+} carcinogenesis,[2,4,5] and many of the cellular pathways altered following Cd^{2+} treatment are associated with oxidative stress.[2,4] In this vein, our results revealed that Cd^{2+} exposure induced significant upregulations of several important antioxidant enzymes (Table 1) and 11 proteins involved in glutathione metabolism. Our quantitative proteomic analysis revealed that Cd^{2+} treatment also induced significant upregulations of DDAH I and DDAH II, two important enzymes involved in the regulation of NO biosynthesis (Table 1). This was accompanied with a concomitant rise in total nitrate/nitrite levels in the cell lysates and culture media (Figure 4 and Figure S3), suggesting that elevated expression of DDAH I and DDAH II contributes to increased NO formation. The latter may give rise to the activation of antioxidant defense systems.[2,4,5]

Elevated antioxidant defense response has been well-documented in a variety of model systems following Cd^{2+} exposure.[2,4] However, relatively little is known about other cellular pathways that may be simultaneously altered in response to Cd^{2+} exposure or their contributions to overall Cd^{2+} toxicity, particularly in mammalian systems. We found that many proteins involved in cellular metabolism pathways, including glycolysis, pentose phosphate pathway, and the citric acid cycle, were also significantly increased following Cd^{2+} treatment (Table 1). The increases in cellular metabolism pathways may help to maintain cellular redox homeostasis upon Cd^{2+} exposure. For instance, the pentose phosphate pathway plays a crucial role in redox regulation via the generation of NADPH, the reductant used to maintain the reduced form of GSH.[29]

Together, our systems-based approach provided integrated information about the cellular pathways altered in response to Cd^{2+} exposure (Figure 5 and Table S4). Our results not only recapitulated some previous findings obtained from disparate approaches of investigation with the use of various in vitro and in vivo models but also provided much more comprehensive coverage of important players (proteins) involved in each individual pathway. In addition, our results suggest that elevated expression of DDAH I and II may contribute to increased formation of NO and augmented generation of ROS following Cd^{2+} exposure. Discovery of the specific biological pathways perturbed by Cd^{2+} exposure in combination with the proteins involved in these pathways may ultimately lead to

development of improved approaches for risk assessment, better prevention and treatment strategies for Cd^{2+} exposure, and robust biomarkers for monitoring Cd^{2+} exposure.

■ ASSOCIATED CONTENT

Supporting Information

Detailed results for all proteins quantified from three independent sets of SILAC experiments; summary of quantification results for all proteins that are signifcantly altered in response to 3 μM Cd^{2+} exposure; significant KEGG pathways identified by DAVID bioinformatics analysis; functional protein-association networks for proteins whose expression levels are significantly altered in response to Cd^{2+} treatment, as revealed by analysis using STRING tool; list of primers used for real-time PCR analysis; trypan blue-exclusion assay for monitoring the viability of GM00637 cells treated for 24 h with different concentrations of Cd^{2+}; quantitative real-time PCR for monitoring the expression levels of HMGCR and FDPS; and total nitrate/nitrite concentrations in IMR-90 human lung fibroblast cells treated with Cd^{2+}. This material is available free of charge via the Internet at http://pubs.acs.org.

■ AUTHOR INFORMATION

Corresponding Author

*Phone: (951) 827-2700. Fax: (951) 827-4713. E-mail: yinsheng.wang@ucr.edu.

Notes

The authors declare no competing financial interest.

■ ACKNOWLEDGMENTS

This research was supported by the National Institutes of Health (R01 ES019873), and John M. Prins was supported by an NRSA T32 institutional training grant (T32 ES018827) and a Postdoctoral Fellowship Award from the California Tobacco-Related Disease Research Program (21FT-0086).

■ ABBREVIATIONS

SILAC, stable isotope labeling by amino acids in cell culture; MS, mass spectrometry; CID, collisionally induced dissociation; HCD, higher-energy collisional dissociation; IMDM, Iscove's modified Dulbecco's medium; EMEM, Eagle's minimum essential medium; PBS, phosphate-buffered saline; FBS, fetal bovine serum; SDS-PAGE, sodium dodecyl sulfate polyacrylamide gel electrophoresis; DDAH, dimethylarginine dimethylaminohydrolase; ROS, reactive oxygen species

■ REFERENCES

(1) Beyersmann, D.; Hartwig, A. Carcinogenic metal compounds: Recent insight into molecular and cellular mechanisms. *Arch. Toxicol.* **2008**, *82*, 493−512.

(2) Joseph, P. Mechanisms of cadmium carcinogenesis. *Toxicol. Appl. Pharmacol.* **2009**, *238*, 272−279.

(3) Chiba, M.; Masironi, R. Toxic and trace elements in tobacco and tobacco smoke. *Bull. W.H.O.* **1992**, *70*, 269−275.

(4) Hartwig, A. Mechanisms in cadmium-induced carcinogenicity: Recent insights. *BioMetals* **2010**, *23*, 951−960.

(5) Liu, J.; Qu, W.; Kadiiska, M. B. Role of oxidative stress in cadmium toxicity and carcinogenesis. *Toxicol. Appl. Pharmacol.* **2009**, *238*, 209−214.

(6) Ong, S. E. The expanding field of SILAC. *Anal. Bioanal. Chem.* **2012**, *404*, 967−976.

(7) Roth, U.; von Roepenack-Lahaye, E.; Clemens, S. Proteome changes in *Arabidopsis thaliana* roots upon exposure to Cd^{2+}. *J. Exp. Bot.* **2006**, *57*, 4003−4013.

(8) Farinati, S.; DalCorso, G.; Bona, E.; Corbella, M.; Lampis, S.; Cecconi, D.; Polati, R.; Berta, G.; Vallini, G.; Furini, A. Proteomic analysis of *Arabidopsis halleri* shoots in response to the heavy metals cadmium and zinc and rhizosphere microorganisms. *Proteomics* **2009**, *9*, 4837−4850.

(9) Kieffer, P.; Planchon, S.; Oufir, M.; Ziebel, J.; Dommes, J.; Hoffmann, L.; Hausman, J. F.; Renaut, J. Combining proteomics and metabolite analyses to unravel cadmium stress-response in poplar leaves. *J. Proteome Res.* **2009**, *8*, 400−417.

(10) Zhu, J. Y.; Huang, H. Q.; Bao, X. D.; Lin, Q. M.; Cai, Z. Acute toxicity profile of cadmium revealed by proteomics in brain tissue of *Paralichthys olivaceus*: Potential role of transferrin in cadmium toxicity. *Aquat. Toxicol.* **2006**, *78*, 127−135.

(11) Chora, S.; Starita-Geribaldi, M.; Guigonis, J. M.; Samson, M.; Romeo, M.; Bebianno, M. J. Effect of cadmium in the clam *Ruditapes decussatus* assessed by proteomic analysis. *Aquat. Toxicol.* **2009**, *94*, 300−308.

(12) Thompson, E. L.; Taylor, D. A.; Nair, S. V.; Birch, G.; Haynes, P. A.; Raftos, D. A. Proteomic discovery of biomarkers of metal contamination in Sydney Rock oysters (*Saccostrea glomerata*). *Aquat. Toxicol.* **2013**, *109*, 202−212.

(13) Dorts, J.; Kestemont, P.; Dieu, M.; Raes, M.; Silvestre, F. Proteomic response to sublethal cadmium exposure in a sentinel fish species, *Cottus gobio*. *J. Proteome Res.* **2013**, *10*, 470−478.

(14) Lau, A. T.; Chiu, J. F. The possible role of cytokeratin 8 in cadmium-induced adaptation and carcinogenesis. *Cancer Res.* **2007**, *67*, 2107−2113.

(15) Zhang, Q.; Zou, P.; Zhan, H.; Zhang, M.; Zhang, L.; Ge, R. S.; Huang, Y. Dihydrolipoamide dehydrogenase and cAMP are associated with cadmium-mediated Leydig cell damage. *Toxicol. Lett.* **2011**, *205*, 183−189.

(16) Zhang, F.; Dai, X.; Wang, Y. 5-Aza-2′-deoxycytidine induced growth inhibition of leukemia cells through modulating endogenous cholesterol biosynthesis. *Mol. Cell. Proteomics* **2012**, *11*, M111.016915-1−M111.016915-8.

(17) Cox, J.; Mann, M. MaxQuant enables high peptide identification rates, individualized p.p.b.-range mass accuracies and proteome-wide protein quantification. *Nat. Biotechnol.* **2008**, *26*, 1367−1372.

(18) Huang, D. W.; Sherman, B. T.; Lempicki, R. A. Systematic and integrative analysis of large gene lists using DAVID bioinformatics resources. *Nat. Protoc.* **2009**, *4*, 44−57.

(19) Franceschini, A.; Szklarczyk, D.; Frankild, S.; Kuhn, M.; Simonovic, M.; Roth, A.; Lin, J.; Minguez, P.; Bork, P.; von Mering, C.; Jensen, L. J. STRING v9.1: Protein-protein interaction networks, with increased coverage and integration. *Nucleic Acids Res.* **2013**, *41*, D808−D815.

(20) Livak, K. J.; Schmittgen, T. D. Analysis of relative gene expression data using real-time quantitative PCR and the $2^{-\Delta\Delta Ct}$ method. *Methods* **2001**, *25*, 402−408.

(21) Dong, X.; Xiong, L.; Jiang, X.; Wang, Y. Quantitative proteomic analysis reveals the perturbation of multiple cellular pathways in jurkat-T cells induced by doxorubicin. *J. Proteome Res.* **2010**, *9*, 5943−5951.

(22) Xiong, L.; Wang, Y. Quantitative proteomic analysis reveals the perturbation of multiple cellular pathways in HL-60 cells induced by arsenite treatment. *J. Proteome Res.* **2010**, *9*, 1129−1137.

(23) Kolluru, G. K.; Tamilarasan, K. P.; Geetha Priya, S.; Durgha, N. P.; Chatterjee, S. Cadmium induced endothelial dysfunction: consequence of defective migratory pattern of endothelial cells in association with poor nitric oxide availability under cadmium challenge. *Cell Biol. Int.* **2006**, *30*, 427−438.

(24) Hassoun, E. A.; Stohs, S. J. Cadmium-induced production of superoxide anion and nitric oxide, DNA single strand breaks and lactate dehydrogenase leakage in J774A.1 cell cultures. *Toxicology* **1996**, *112*, 219−226.

(25) Ramirez, D. C.; Martinez, L. D.; Marchevsky, E.; Gimenez, M. S. Biphasic effect of cadmium in non-cytotoxic conditions on the

secretion of nitric oxide from peritoneal macrophages. *Toxicology* **1999**, *139*, 167−177.
(26) Dayoub, H.; Achan, V.; Adimoolam, S.; Jacobi, J.; Stuehlinger, M. C.; Wang, B. Y.; Tsao, P. S.; Kimoto, M.; Vallance, P.; Patterson, A. J.; Cooke, J. P. Dimethylarginine dimethylaminohydrolase regulates nitric oxide synthesis: Genetic and physiological evidence. *Circulation* **2003**, *108*, 3042−3047.
(27) Board, P. G.; Menon, D. Glutathione transferases, regulators of cellular metabolism and physiology. *Biochim. Biophys. Acta* **2013**, *1830*, 3267−3288.
(28) DeBerardinis, R. J.; Lum, J. J.; Hatzivassiliou, G.; Thompson, C. B. The biology of cancer: Metabolic reprogramming fuels cell growth and proliferation. *Cell Metab.* **2008**, *7*, 11−20.
(29) Kletzien, R. F.; Harris, P. K.; Foellmi, L. A. Glucose-6-phosphate dehydrogenase: A "housekeeping" enzyme subject to tissue-specific regulation by hormones, nutrients, and oxidant stress. *FASEB J.* **1994**, *8*, 174−181.
(30) Arthur, J. R. The glutathione peroxidases. *Cell. Mol. Life Sci.* **2000**, *57*, 1825−1835.
(31) Tong, L. Acetyl-coenzyme A carboxylase: Crucial metabolic enzyme and attractive target for drug discovery. *Cell. Mol. Life Sci.* **2005**, *62*, 1784−1803.
(32) Espenshade, P. J.; Hughes, A. L. Regulation of sterol synthesis in eukaryotes. *Annu. Rev. Genet.* **2007**, *41*, 401−427.
(33) Lunt, S. Y.; Vander Heiden, M. G. Aerobic glycolysis: Meeting the metabolic requirements of cell proliferation. *Annu. Rev. Cell Dev. Biol.* **2011**, *27*, 441−464.
(34) Faiz, H.; Conjard-Duplany, A.; Boghossian, M.; Martin, G.; Baverel, G.; Ferrier, B. Cadmium chloride inhibits lactate gluconeogenesis in isolated human renal proximal tubules: A cellular metabolomic approach with ^{13}C-NMR. *Arch. Toxicol.* **2011**, *85*, 1067−1077.
(35) Lopez-Millan, A. F.; Sagardoy, R.; Solanas, M.; Abadia, A.; Abadia, J. Cadmium toxicity in tomato (*Lycopersicon esculentum*) plants grown in hydroponics. *Environ. Exp. Bot.* **2009**, *65*, 376−385.
(36) Prozialeck, W. C.; Lamar, P. C.; Lynch, S. M. Cadmium alters the localization of N-cadherin, E-cadherin, and beta-catenin in the proximal tubule epithelium. *Toxicol. Appl. Pharmacol.* **2003**, *189*, 180−195.